Pergamon

Int. J. Solids Structures Vol. 33, No. 3, pp. 375–398, 1996

0020–7683/96 $9.50 + .00

0020–7683(95)00042–9

PREDICTIONS OF DEFLECTION AND FIRST-PLY FAILURE LOAD OF THIN LAMINATED COMPOSITE PLATES VIA THE FINITE ELEMENT APPROACH

T. Y. KAM, H. F. SHER and T. N. CHAO
Mechanical Engineering Department, National Chiao Tung University, Hsin-Chu 30050, Taiwan, Republic of China

and

R. R. CHANG
Mechanical Engineering Department, China Junior College of Technology, Taipei 11522, Taiwan, Republic of China

(*Received* 5 *April* 1994; *in revised form* 16 *February* 1995)

Abstract—A nonlinear finite element method, which is based on the von Karman–Mindlin plate theory and the principle of minimum total potential energy, is used to study the deformation and first-ply failure of thin laminated composite plates. The load–displacement curves of a number of laminated composite plates are determined using the proposed finite element method. Stresses obtained from the linear and nonlinear finite element analyses are used to determine, respectively, the linear and nonlinear first-ply failure loads of the laminated plates based on several phenomenological failure criteria. The accuracy of the finite element results is then verified by comparison with the available experimental data. It has been found that good agreement between the finite element and experimental load–strain curves before first-ply failure is observed. If the reduction in plate stiffness induced by failure of plies is taken into account in the finite element model, close agreement between finite element and experimental load–displacement curves from first-ply failure up to total failure may be obtained. Regarding the prediction of the first-ply failure load, it has been found that some of the phenomenological failure criteria may yield results of consistent accuracy for the laminated composite plates under consideration. Nevertheless, accurate prediction of the failure process after first-ply failure is still intractable. Hence, for reliability assurance further research on failure analysis of laminated composite plates subject to transverse loading is needed.

1. INTRODUCTION

Because of their high stiffness/strength to weight ratios and many other superior properties, laminated composite materials have been widely used in the construction of mechanical, aerospace, marine and automotive structures which, in general, require high reliability. For reliability assurance, prediction of the failure process of laminated composite structures and the maximum loads that the structures can withstand before failure occurs has thus become an important research topic. In particular, the first-ply failure analysis of laminated composite plates has been actively investigated in recent years. A vast literature has been devoted to matrix cracking and first-ply failure analysis of laminated composite plates subject to in-plane forces [e.g. Hahn and Tsai (1974), Wang and Crossman (1980), and Dvorak and Laws (1987)]. Extensive testing has also been conducted to study the formation of matrix cracks and stiffness reduction in composite laminates (Garrett and Bailey, 1977; Highsmith and Reifsnider, 1982). On the other hand, the mechanical behavior and first-ply failure load of laminated composite plates subjected to transverse loads has also been studied by a number of researchers. For example, Turvey (1980a,b, 1982, 1989) used analytical and numerical methods to study the linear and nonlinear first-ply failure loads of simply supported symmetrically and antisymmetrically laminated composite plates based on the classical and Mindlin laminated plate theory; Reddy and his associates (1987, 1992) used the finite element method to calculate the linear and nonlinear first-ply failure loads of laminated composite plates based on several phenomenological failure criteria; Kam and associates (1992, 1993) studied the first-ply failure probabilities of linear and nonlinear

laminated composite plates. As for deflection analysis, a number of researchers have investigated the nonlinear deflection of laminated composite plates using various methods (Reddy and Chao, 1982; Kuppusamy and Reddy, 1984; Dumir and Bhaskar, 1988). Most of the previous works on deflection or first-ply failure analysis of laminates under transverse loads, however, have been limited to theoretical investigations and few of them have been verified by experimental data. It is well known that laminated composite plates subject to static loads may experience large deflection during the failure process. In particular, for thin laminated composite plates (side-to-thickness ratio $a/h > 70$), the load–deflection relation may be nonlinear even before the occurrence of first-ply failure. For moderately thick laminated plates, the load–deflection relation usually becomes nonlinear after first-ply failure. The nonlinear effects, therefore, must be taken into account if more accurate predictions of the mechanical behavior and ultimate strength of laminated composite plates are desired. In this paper, a nonlinear finite element method based on the von Karman–Mindlin plate theory is used to study the nonlinear deflection and first-ply failure load of laminated composite plates subject to transverse loading. To validate the applicability of the present method to thin laminated composite plates, an eight-node element of the serendipity family and nine-node Lagrangian elements with different numerical integration rules are used separately to construct the load–displacement curves of several laminated composite plates loaded by an equivalent center point force and the finite element results are compared with those obtained from experiment. Stresses obtained with the linear and nonlinear finite element analyses of the plates are used to evaluate, respectively, the linear and nonlinear first-ply failure loads of the plates based on several phenomenological failure criteria. The capabilities of the failure criteria in predicting first-ply failure load are investigated by comparing the linear and nonlinear first-ply failure loads determined with the finite element analyses with those obtained from experiment using an acoustic emission technique. A hypothetical stiffness reduction model is proposed to study the deflection and the ultimate strength of the damaged laminated composite plates. The capabilities of the proposed stiffness reduction model in predicting load–displacement curves and ultimate strengths of the laminated plates are demonstrated by means of two examples.

2. NONLINEAR THEORY OF LAMINATED COMPOSITE PLATES

The laminated composite plate under consideration is made of a number of orthotropic layers of equal thickness. The x and y coordinates of the plate are taken in the midplane of the plate which has area $a \times b$ and thickness h. In order to have a theory suitable for both thin and moderately thick laminated plates, the displacement field is assumed to be of the form

$$\begin{aligned} u_x(x,y,z) &= u_0(x,y) + z \cdot \psi_x(x,y) \\ u_y(x,y,z) &= v_0(x,y) + z \cdot \psi_y(x,y) \\ u_z(x,y,z) &= w(x,y), \end{aligned} \tag{1}$$

where u_x, u_y, u_z are the displacements in the x, y, z directions, respectively, u_0, v_0, w the associated midplane displacements, and ψ_x and ψ_y the shear rotations. The strain–displacement relations in the von Karman plate theory can be expressed in the form

$$\varepsilon_x = \frac{\partial u_0}{\partial x} + \frac{1}{2}\left(\frac{\partial w}{\partial x}\right)^2 + z\frac{\partial \psi_x}{\partial x} = \varepsilon_x^0 + z\kappa_x$$

$$\varepsilon_y = \frac{\partial v_0}{\partial y} + \frac{1}{2}\left(\frac{\partial w}{\partial y}\right)^2 + z\frac{\partial \psi_y}{\partial y} = \varepsilon_y^0 + z\kappa_y$$

$$\varepsilon_s = \frac{\partial u_0}{\partial y} + \frac{\partial v_0}{\partial x} + \frac{\partial w}{\partial x}\frac{\partial w}{\partial y} + z\left(\frac{\partial \psi_x}{\partial y} + \frac{\partial \psi_y}{\partial x}\right) = \varepsilon_s^0 + z\kappa_s$$

$$\varepsilon_5 = \psi_x + \frac{\partial w}{\partial x}, \quad \varepsilon_4 = \psi_y + \frac{\partial w}{\partial y}, \tag{2}$$

where $\varepsilon_i^0 (i = x, y, s)$ are in-plane strains, ε_j $(j = 4,5)$ are transverse shear strains, and κ_i are bending curvatures. It is noted that in case of a linear analysis of the plate, the nonlinear terms, i.e.

$$\left(\frac{\partial w}{\partial x}\right)^2 \quad \text{and} \quad \frac{\partial w}{\partial x} \cdot \frac{\partial w}{\partial y},$$

in the above equations can be neglected. The associated Piola–Kirchoff stress vector σ is

$$\sigma = [\sigma_x, \sigma_y, \sigma_s, \sigma_5, \sigma_4]^T. \tag{3}$$

The constitutive equations for the plate can be written as

$$\begin{Bmatrix} N_i \\ M_i \end{Bmatrix} = \begin{bmatrix} A_{ij} & B_{ij} \\ B_{ij} & D_{ij} \end{bmatrix} \begin{Bmatrix} \varepsilon_j^0 \\ \kappa_j \end{Bmatrix} \quad (i,j = x, y, s)$$

and

$$\begin{Bmatrix} Q_2 \\ Q_1 \end{Bmatrix} = \begin{bmatrix} \bar{A}_{44} & \bar{A}_{45} \\ \bar{A}_{45} & \bar{A}_{55} \end{bmatrix} \begin{Bmatrix} \varepsilon_4 \\ \varepsilon_5 \end{Bmatrix} \tag{4a}$$

or in matrix form,

$$\begin{Bmatrix} \mathbf{N} \\ \mathbf{M} \end{Bmatrix} = \begin{bmatrix} \mathbf{A} & \mathbf{B} \\ \mathbf{B} & \mathbf{D} \end{bmatrix} \begin{Bmatrix} \boldsymbol{\varepsilon}^0 \\ \boldsymbol{\kappa} \end{Bmatrix}$$

and

$$\mathbf{Q} = \bar{\mathbf{A}}\boldsymbol{\gamma}. \tag{4b}$$

Here N_i, M_i, Q_1 and Q_2 are the stress resultants defined by

$$(N_i, M_i) = \int_{-h/2}^{h/2} (1, z)\sigma_i \, dz, \quad (Q_1, Q_2) = \int_{-h/2}^{h/2} (\sigma_5, \sigma_4) \, dz. \tag{5}$$

The A_{ij}, B_{ij}, D_{ij} $(i,j = x, y, s)$ and $\bar{A}_{ij}$ $(i,j = 4, 5)$ are the in-plane, bending in-plane coupling, bending or twisting, and thickness–shear stiffness coefficients, respectively:

$$(A_{ij}, B_{ij}, D_{ij}) = \sum_{m=1}^{NL} \int_{z_m}^{z_{m+1}} Q_{ij}^{(m)}(1, z, z^2) \, dz \quad (i,j = x, y, s)$$

$$\bar{A}_{ij} = \sum_{m=1}^{NL} \int_{z_m}^{z_{m+1}} k_\alpha k_\beta Q_{ij}^{(m)} \, dz, \quad (i,j = 4,5; \alpha = 6-i, \beta = 6-j) \tag{6}$$

where z_m denotes the distance from the midplane to the lower surface of the mth layer, NL is the total number of layers, Q_{ij} are material constants, and k_α are the shear correction coefficients which are set as $k_1 = k_2 = \sqrt{\frac{5}{6}}$.

The basis of the formulation of the governing equations of the plate is the principle of minimum total potential energy in which the total potential energy π is expressed as the sum of strain energy U and potential energy V, i.e.

$$\pi = U + V, \tag{7}$$

where

$$U = \frac{1}{2}\int_v \boldsymbol{\varepsilon}^{\mathrm{T}}\boldsymbol{\sigma}\,\mathrm{d}v \tag{8a}$$

and

$$V = -\int_\Omega q(x,y)w(x,y)\,\mathrm{d}\Omega, \tag{8b}$$

where v is plate volume, $q(x,y)$ distributed load intensity, and Ω plate area.

In view of the above strain–displacement relations and constitutive equations, the plate strain energy can be expressed as a function of the five unknown mid-plane displacements $(u_0, v_0, w, \psi_x, \psi_y)$. After integrating through the plate thickness, the strain energy becomes

$$U = \frac{1}{2}\int\int [\boldsymbol{\varepsilon}^{0\mathrm{T}}\mathbf{A}\boldsymbol{\varepsilon}^0 + 2\boldsymbol{\varepsilon}^{0\mathrm{T}}\mathbf{B}\boldsymbol{\kappa} + \boldsymbol{\kappa}^{\mathrm{T}}\mathbf{D}\boldsymbol{\kappa} + \boldsymbol{\gamma}^{\mathrm{T}}\bar{\mathbf{A}}\boldsymbol{\gamma}]\,\mathrm{d}x\,\mathrm{d}y. \tag{9}$$

The first variation of eqn (7) gives

$$\delta\pi = \delta(U+V) = 0. \tag{10}$$

3. FINITE ELEMENT FORMULATION

Consider the laminated composite plate discretized into NE elements. The strain energy and potential energy of the plate are expressed, respectively, as

$$U = \sum_{i=1}^{NE} U_{\mathrm{e}} = \frac{1}{2}\sum_{i=1}^{NE}\left\{\int_{\Omega_{\mathrm{e}}} [\boldsymbol{\varepsilon}^{0\mathrm{T}}\mathbf{A}\boldsymbol{\varepsilon}^0 + 2\boldsymbol{\varepsilon}^{0\mathrm{T}}\mathbf{B}\boldsymbol{\kappa} + \boldsymbol{\kappa}^{\mathrm{T}}\mathbf{D}\boldsymbol{\kappa} + \boldsymbol{\gamma}^{\mathrm{T}}\bar{\mathbf{A}}\boldsymbol{\gamma}]\,\mathrm{d}\Omega\right\}_i \tag{11}$$

and

$$V = \sum_{i=1}^{NE}\left[\int_{\Omega_{\mathrm{e}}} q(x,y)w(x,y)\,\mathrm{d}\Omega\right]_i, \tag{12}$$

where Ω_e, U_e are the element area and strain energy, respectively.

The mid-plane displacements $(u_0, v_0, w, \psi_x, \psi_y)$ within an element are given as functions of $5 \times q$ discrete nodal displacements and in matrix form they are expressed as

$$\mathbf{u} = \sum_{i=1}^{q} [\Phi_i \mathbf{I}]\nabla_{ei} = \boldsymbol{\Phi}\tilde{\nabla}_{\mathrm{e}}, \tag{13}$$

where q is the number of nodes of the element; Φ_i are the shape functions; $\mathbf{I}$ is a 5×5 unit matrix; $\boldsymbol{\Phi}$ is the shape function matrix; $\tilde{\nabla}_{\mathrm{e}} = \{\nabla_{\mathrm{e}1}, \nabla_{\mathrm{e}2}, \ldots, \nabla_{\mathrm{e}q}\}^{\mathrm{T}}$; the nodal displacements ∇_{ei} at a node are

$$\mathbf{V}_{ei} = \{u_{0i}, v_{0i}, w_i, \psi_{xi}, \psi_{yi}\}^{\mathrm{T}}, \quad i = 1, \ldots, q. \tag{14}$$

The substitution of eqns (11)–(13) into (10) yields

$$\delta\pi = \sum_{i=1}^{NE} [\delta\tilde{\mathbf{V}}_e^{\mathrm{T}} \mathbf{F}_e(\tilde{\mathbf{V}}_e)]_i - \sum_{i=1}^{NE} [\delta\tilde{\mathbf{V}}_e^{\mathrm{T}} \mathbf{P}_e]_i = 0, \tag{15}$$

where $\mathbf{F}_e(\tilde{\mathbf{V}}_e)$, $\mathbf{P}_e$ are the element internal and nodal force vectors, respectively. The element internal force vector is obtained as

$$\mathbf{F}_e(\tilde{\mathbf{V}}_e) = \frac{\partial U_e}{\partial \tilde{\mathbf{V}}_e}. \tag{16}$$

The terms in $\mathbf{F}_e$ are expressed explicitly in Appendix A. Using the standard finite element approach to add the contributions of all the elements in the domain and noting that the variations of nodal displacements are arbitrary, the equilibrium equations of the plate can be obtained from eqn (15) as

$$\mathbf{F}(\mathbf{V}) - \mathbf{P} = 0, \tag{17}$$

where $\mathbf{F}$, $\mathbf{V}$, $\mathbf{P}$, are global internal force, nodal displacement and nodal force vectors, respectively. Since the above equations are nonlinear, an incremental-iterative loading procedure is adopted to construct the load–displacement curve of the plate. Express eqn (17) in a truncated Taylor series as

$$\mathbf{F}(\mathbf{V}^n) - \mathbf{P} + \frac{\partial \mathbf{F}(\mathbf{V}^n)}{\partial \mathbf{V}} \Delta\mathbf{V}^n \cong 0, \tag{18}$$

where the superscript n denotes iteration number.

The increments in nodal displacements are obtained from the above equation as

$$\Delta\mathbf{V}^n = -\left[\frac{\partial \mathbf{F}(\mathbf{V}^n)}{\partial \mathbf{V}}\right]^{-1} \cdot [\mathbf{F}(\mathbf{V}^n) - \mathbf{P}], \tag{19}$$

where $[\cdot]^{-1}$ denotes the inverse of the matrix in the bracket.

The updated nodal displacements are

$$\mathbf{V}^{n+1} = \mathbf{V}^n + \Delta\mathbf{V}^n \tag{20}$$

Define the structural tangent stiffness matrix $\mathbf{K}_T$ and residual force vector ψ, respectively, as

$$\mathbf{K}_T = \frac{\partial \mathbf{F}}{\partial \mathbf{V}} \tag{21}$$

and

$$\psi = \mathbf{F} - \mathbf{P}. \tag{22}$$

In view of the above equations, eqn (19) can be rewritten as

$$\Delta \mathbf{V}^n = -\mathbf{K}_T(\mathbf{V}^n)^{-1}\boldsymbol{\psi}(\mathbf{V}^n). \tag{23}$$

The solution converges when the norm of the residual force vector is less than a prescribed value, say, 10^{-3}. It is noted that the structural tangent stiffness matrix $\mathbf{K}_T$ in eqn (21) is obtained by assembling all the element tangent stiffness matrices $\mathbf{K}_{ei}$, $i = 1, \ldots, NE$.

$$\mathbf{K}_T = \sum_{i=1}^{NE} [\mathbf{a}^T \mathbf{K}_e \mathbf{a}]_i \tag{24}$$

with

$$\mathbf{K}_e = \frac{\partial \mathbf{F}_e}{\partial \tilde{\mathbf{V}}_e} = \frac{\partial^2 U_e}{\partial \tilde{\mathbf{V}}_e^T \partial \tilde{\mathbf{V}}_e}, \tag{25}$$

where $\mathbf{a}$ is a congruent transformation matrix.

The terms in $\mathbf{K}_e$ are listed in Appendix B. In the finite element formulation, one of the following three kinds of element may be used to construct the element tangent stiffness matrix: (i) a quadratic ($q = 8$) element of the serendipity family with reduced integration using the 2×2 Gauss rule (designated as Element A); (ii) a nine-node Lagrangian element with reduced integration using the 2×2 Gauss rule (designated as Element B); (iii) a nine-node Lagrangian element with integration using the 3×3 Gauss rule for computing the in-plane and flexural stiffnesses and the reduced 2×2 Gauss rule for transverse shear (designated as Element C). In the case of linear finite element analysis, the tangent stiffness matrix $\mathbf{K}_T$ becomes constant and the equilibrium equations of eqn (17) can be solved directly by using the standard finite element approach.

4. FIRST-PLY FAILURE ANALYSIS

The load that makes the first-ply fail is calculated based on seven different failure criteria, five of which are degenerate cases of the tensor polynomial criterion proposed by Tsai and Wu (1971). The limit state equations of the seven failure criteria are expressed as follows (Reddy and Pandey, 1987):

(i) Maximum stress criterion

The maximum stress criterion states that the stresses in the principal material directions must be less than the respective strengths, otherwise fracture is said to have occurred, that is,

$$\sigma_1 < X_T; \quad \sigma_3 < Z_T; \quad \sigma_5 < S; \quad \sigma_2 < Y_T; \quad \sigma_4 < R; \quad \sigma_6 < S, \tag{26}$$

where σ_1, σ_2, σ_3 are normal stress components, σ_4, σ_5, σ_6 are shear stress components, X_T, Y_T, Z_T are the lamina normal strengths in the 1, 2, 3 directions and R, S are the shear strengths in the 23 and 12 planes, respectively. When σ_1, σ_2, σ_3 are of a compressive nature they should be compared with X_C, Y_C, Z_C which are normal strengths in compression along the 1, 2, 3 directions, respectively.

(ii) Maximum strain criterion

Failure of the material is assumed to occur if any of the following conditions are satisfied:

$$\varepsilon_1 > X_{\varepsilon T}; \quad \varepsilon_3 > Z_{\varepsilon T}; \quad \varepsilon_5 > S_\varepsilon; \quad \varepsilon_2 > Y_{\varepsilon T}; \quad \varepsilon_4 > R_\varepsilon; \quad \varepsilon_6 > S_\varepsilon, \tag{27}$$

where ε_1, ε_2, ε_3 are the normal strain components, ε_4, ε_5 and ε_6 are shear strain components, $X_{\varepsilon T}, \ldots, R_\varepsilon$ are strain strengths. When ε_1, ε_2, ε_3 are negative, they should be compared with $X_{\varepsilon C}$, $Y_{\varepsilon C}$, $Z_{\varepsilon C}$, respectively, which are normal strain strengths in compression.

(iii) Polynomial type maximum stress criterion
The polynomial type maximum stress criterion can be expressed as

$$(\sigma_1 - X_T)(\sigma_1 + X_C)(\sigma_2 - Y_T)(\sigma_2 + Y_C)(\sigma_3 - Z_T)(\sigma_3 + Z_C) \times (\sigma_4 - R)(\sigma_4 + R)(\sigma_5 - S)(\sigma_5 + S)(\sigma_6 - S)(\sigma_6 + S) = 0. \quad (28)$$

(iv) Polynomial type maximum strain criterion
Failure of the material is assumed to occur if the following condition is satisfied:

$$(\varepsilon_1 - X_{\varepsilon T})(\varepsilon_1 + X_{\varepsilon C})(\varepsilon_2 - Y_{\varepsilon T})(\varepsilon_2 + Y_{\varepsilon C})(\varepsilon_3 - Z_{\varepsilon T})(\varepsilon_3 + Z_{\varepsilon C}) \times (\varepsilon_4 - R_\varepsilon)(\varepsilon_4 + R_\varepsilon)(\varepsilon_5 - S_\varepsilon)(\varepsilon_5 + S_\varepsilon)(\varepsilon_6 - S_\varepsilon)(\varepsilon_6 + S_\varepsilon) = 0. \quad (29)$$

(v) Hoffman's criterion
The Hoffman's criterion can be expressed as

$$\frac{1}{2}\left(-\frac{1}{X_T X_C} + \frac{1}{Y_T Y_C} + \frac{1}{Z_T Z_C}\right)(\sigma_2 - \sigma_3)^2 + \frac{1}{2}\left(\frac{1}{X_T X_C} - \frac{1}{Y_T Y_C} + \frac{1}{Z_T Z_C}\right)(\sigma_3 - \sigma_1)^2 + \frac{1}{2}\left(\frac{1}{X_T X_C} + \frac{1}{Y_T Y_C} - \frac{1}{Z_T Z_C}\right)(\sigma_1 - \sigma_2)^2 + \left(\frac{1}{X_T} - \frac{1}{X_C}\right)\sigma_1 + \left(\frac{1}{Y_T} - \frac{1}{Y_C}\right)\sigma_2 + \left(\frac{1}{Z_T} - \frac{1}{Z_C}\right)\sigma_3 + \left(\frac{\sigma_4}{R}\right)^2 + \left(\frac{\sigma_5}{S}\right)^2 + \left(\frac{\sigma_6}{S}\right)^2 \geqslant 1. \quad (30)$$

(vi) Tsai–Hill criterion
The Tsai–Hill criterion can be expressed as

$$\left(\frac{\sigma_1}{X}\right)^2 + \left(\frac{\sigma_2}{Y}\right)^2 + \left(\frac{\sigma_3}{Z}\right)^2 - \left(\frac{1}{X^2} + \frac{1}{Y^2} - \frac{1}{Z^2}\right)\sigma_1\sigma_2 - \left(-\frac{1}{X^2} + \frac{1}{Y^2} + \frac{1}{Z^2}\right)\sigma_2\sigma_3 - \left(\frac{1}{X^2} - \frac{1}{Y^2} + \frac{1}{Z^2}\right)\sigma_1\sigma_3 + \left(\frac{\sigma_4}{R}\right)^2 + \left(\frac{\sigma_5}{S}\right)^2 + \left(\frac{\sigma_6}{S}\right)^2 \geqslant 1. \quad (31)$$

The values of X, Y, Z are taken as either X_T, Y_T and Z_T or as X_C, Y_C and Z_C depending upon the sign of σ_1, σ_2 and σ_3, respectively.

(vii) Tsai–Wu criterion
The Tsai–Wu criterion can be expressed as

$$F_i\sigma_i + F_{ij}\sigma_i\sigma_j \geqslant 1, \quad (32)$$

where

$$F_1 = \frac{1}{X_T} - \frac{1}{X_C}; \quad F_2 = \frac{1}{Y_T} - \frac{1}{Y_C}; \quad F_3 = \frac{1}{Z_T} - \frac{1}{Z_C}$$

$$F_{11} = \frac{1}{X_T X_C}; \quad F_{22} = \frac{1}{Y_T Y_C}; \quad F_{33} = \frac{1}{Z_T Z_C}$$

$$F_{44} = \frac{1}{R^2}; \quad F_{55} = \frac{1}{S^2}; \quad F_{66} = \frac{1}{S^2}$$

$$F_{12} = -\frac{1}{2\sqrt{X_T X_C Y_T Y_C}}; \quad F_{13} = -\frac{1}{2\sqrt{X_T X_C Z_T Z_C}}; \quad F_{23} = -\frac{1}{2\sqrt{Y_T Y_C Z_T Z_C}}. \quad (33)$$

In the above failure criteria, the contribution of normal stress σ_3 is in general small compared to the other stress components so that its effects have been neglected. The shear strengths in the 12 and 13 planes are assumed to be the same. The stresses determined from the linear and nonlinear displacement fields are used to compute, respectively, the linear and nonlinear first-ply failure loads. The determination of the nonlinear first-ply failure load is accomplished via an incremental–iterative scheme (Reddy and Reddy, 1992).

5. STIFFNESS REDUCTION OF COMPOSITE LAMINATES

The stiffness of a laminated composite plate will decrease when failure of plies occurs. Recently a number of stiffness degradation models have been proposed for studying damage in composite laminates (Hahn and Tsai, 1974; Laws *et al.*, 1983; Talreja, 1985; Chang and Chang, 1987). For instance, Talreja (1985) investigated stiffness degradation of composite laminates via a continuum damage characterization approach. Chang and associates (1987, 1989) used a phenomenological failure criterion to study stiffness degradation of laminated composite structures. On the other hand, Cantwell and Morton (1985) studied the influence of target bending stiffness on low velocity impact damage in CFRP laminates using a drop-weight tester. Target stiffness was a dominant parameter and controlled the mode of fracture. At low velocities, flexible targets responded primarily by bending which generated high tensile stresses in the lowest ply. This caused matrix cracks in the lowest ply, which were deflected at the lowest interface to form a delamination, which in turn was deflected by matrix cracks in the layer above, and the process repeated itself. As for thin cross-ply plates indented by a rigid spherical head statically, it is postulated that delamination has insignificant effects on the global behavior of the plates and matrix cracking is the major cause of laminate stiffness reduction before the final stage of the failure process. At the final stage the contribution of fiber breakage becomes important and the breakage of fibers may finally lead to the total collapse of the plates or the penetration of the indentor through plate thickness. Herein, a simple hypothetical stiffness reduction model is proposed to study the deflection of damaged laminated composite plates using the maximum stress failure criterion which can characterize failure modes. As observed in the load controlled indentation test of cross-ply plates, when matrix cracking occurs in a ply, a crack of moderately large size will occur in the fiber direction owing to a sudden release of fracture energy and redistribution of stresses in the damaged plate. Since the determination of exact crack size is a difficult task if not intractable, it is assumed that though generally it may not be valid for laminated composite plates under bending, once a matrix crack forms it will span the whole length of the plate. Hence, based on the maximum stress failure criterion, stresses at the integration points in each element are used to identify the occurrences of failure and determine the degradation of material moduli in the failed plies. If the stress component in the fiber direction (σ_1) of a ply at an element integration point reaches its limit value (fiber failure mode), all the moduli of the ply at that integration point are set to zero. On the other hand, if matrix fracture in a ply induced by either transverse stress (σ_2) or shear stress (σ_6) occurs at an element integration point (matrix failure mode), the crack is assumed to span the whole length of the ply to form a crack line and the transverse Young's modulus (E_2), the shear modulus (G_{12}), the transverse shear modulus (G_{23}) and the Poisson's ratios (ν_{12}, ν_{23}) of the ply at all the element integration points of the elements passed through by the crack line are treated as zero. The effects of transverse shear stresses (σ_4 and σ_5) are small for thin plates and thus will not be included in the stiffness reduction model. The updated layerwise material moduli are then used to modify the element stiffness matrices of the damaged laminated composite plate. A schematic sketch of the stiffness reduction model is shown in Fig. 1.

6. EXPERIMENTAL VERIFICATION

The capability of the proposed finite element method in predicting deflection and first-ply failure load of laminated composite plates will be demonstrated by comparing the finite element results with available experimental results. Four types of centrally loaded laminated

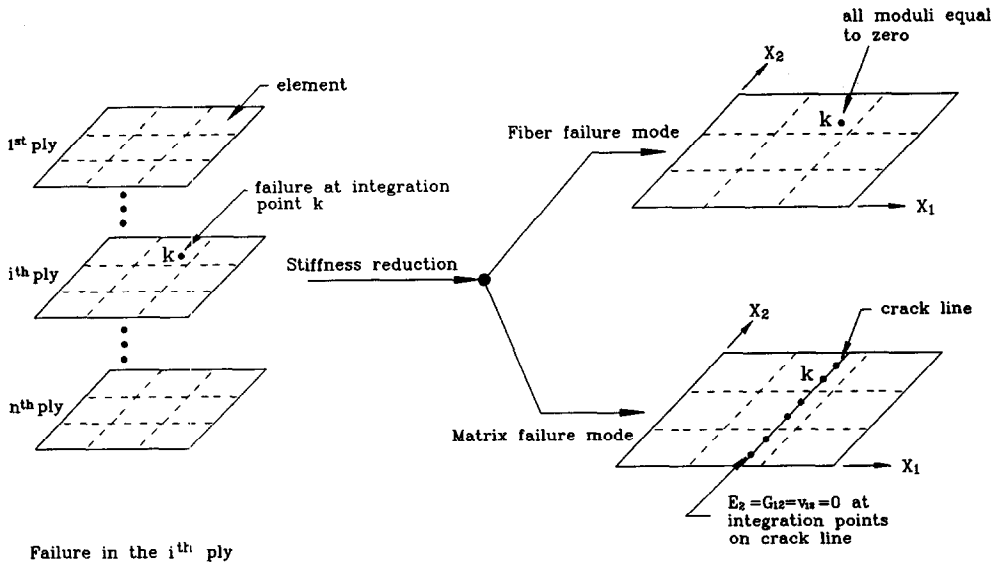

Fig. 1. Stiffness reduction model.

Table 1. Material properties of graphite/epoxy (Q-1115)

Material constants		Strengths			
E_1	142.50 Gpa	X_T	2193.5 Mpa	$X_{\varepsilon T}$	0.015393
E_2	9.79 Gpa	X_C	2457.0 Mpa	$X_{\varepsilon C}$	0.017242
E_3	9.79 Gpa	$Y_T = Z_T$	41.3 Mpa	$Y_{\varepsilon T} = Z_{\varepsilon T}$	0.004128
$G_{12} = G_{13}$	4.72 Gpa	$Y_C = Z_C$	206.8 Mpa	$Y_{\varepsilon C} = Z_{\varepsilon C}$	0.021124
G_{23}	1.192 Gpa	R	61.28 Mpa	R_ε	0.051409
$v_{12} = v_{13}$	0.27	$S = T$	78.78 Mpa	$S_\varepsilon = T_\varepsilon$	0.016691
v_{23}	0.25				

composite square plates of various lamination arrangements and side-to-thickness ratios were tested to failure (Kam, 1993; Kam and Sher, 1995). The laminated composite plates were made of graphite/epoxy (Q-1115) prepreg tapes supplied by the Toho Co., Japan. The material properties were determined from experiments conducted in accordance with the relevant ASTM standards (1990) and are given in Table 1. The experimental apparatus consisted of a 10-ton Instron testing machine, an acoustic emission (AE) system (AMS3) with two AE sensors, a displacement gauge (LVDT), a data acquisition system, a steel load applicator with a spherical head, and a fixture for clamping a specimen. A schematic description of the experimental setup is shown in Fig. 2. The dimensions of the laminated plates and the load applicator are given in Table 2. The fixture was made up of two square steel frames. During testing, the laminated plate was partially clamped by the two steel frames which were connected together by four bolts. It is noted that the clamping method allowed in-plane movements but not rotations at the edges of the laminated plate during loading. The contact areas between the composite laminate and the steel plates were also lubricated to reduce frictional effects. A stroke control approach was adopted in constructing the load-deflection relation for the laminated plate. The loading rate was slow enough for inertia effects to be neglected. During loading, the displacement gauge and data acquisition system recorded center deflections so that the load–displacement curve of the laminated plate could be determined. In addition, two acoustic emission sensors were used to measure the stress waves released at the AE sources in the laminated plate. The measured acoustic emissions were converted by the AMS3 (AE) system to a set of signal describers such as peak amplitude, energy, rise time and duration which were then used to identify the first-ply failure load of the laminated plate (Kam and Sher, 1995). For example, Fig. 3 shows the energy-applied load diagram for a $[0°/90°/0°/90°]_s$ plate produced by the AMS3

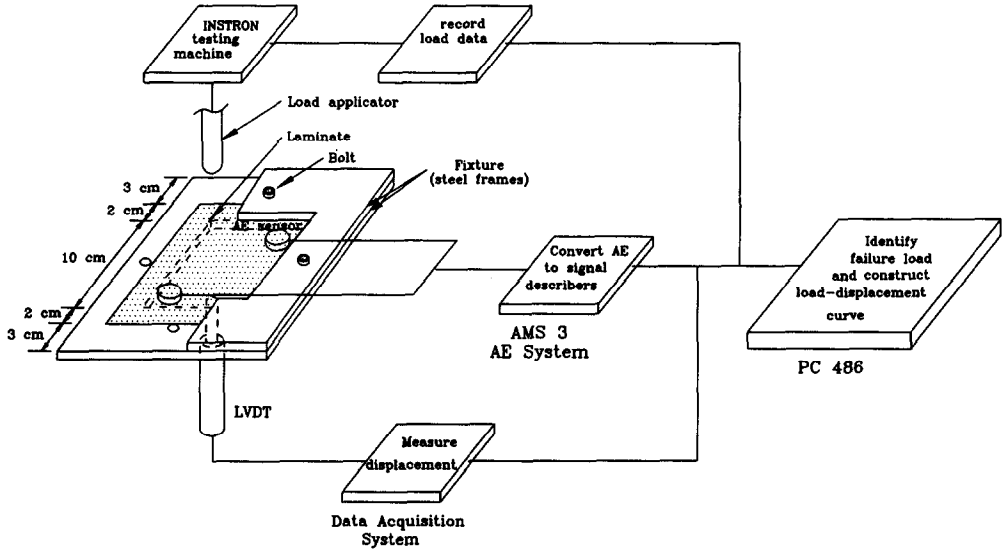

Fig. 2. A schematic description of the experimental setup.

Table 2. Properties of laminated plates and load applicator

Plate	Values
Length (a)	100 mm
Ply thickness (h_i)	0.155 mm
Lamination	$[0°/90°/0°/90°]_s$, $[0_2°/90_2°]_s$, $[0_2°/90°]_s$, $[0°/90°]_s$
Load applicator radius r	5.0 mm

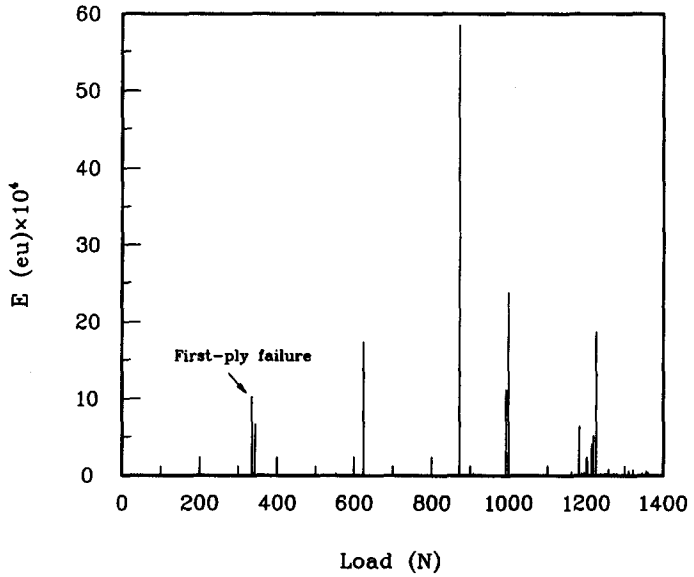

Fig. 3. Energy vs. load produced by AMS3 acoustic emission system for a $[0°/90°/0°/90°]_s$ plate.

system. The first-ply failure load of the plate is determined by identifying the first major energy rise as indicated in Fig. 3.

7. NUMERICAL EXAMPLES AND DISCUSSION

The aforementioned nonlinear finite element method is first used to study the deflection of several simply supported or clamped rectangular thin laminated composite plates with

Table 3. Properties of composite laminates subject to uniform load

Material properties	E_1	E_2	$G_{12} = G_{13}$	G_{23}	$\nu_{12} = \nu_{13}$	ν_{23}	h_i (ply thickness)
Values	132.5 Gpa	10.8 Gpa	5.7 Gpa	3.4 Gpa	0.24	0.49	0.127 mm
Strengths	X_T	X_C	$Y_T = Z_T$	$Y_C = Z_C$	R	$S = T$	
Values	1515 Mpa	1697 Mpa	43.8 Mpa	43.8 Mpa	67.6 Mpa	86.9 Mpa	
Plate	Lamination scheme						
I	$(45°/-45°/90°/0°/45°/90°/-45°/0°)_s$						
II	$(45°/-45°/0°/90°/45°/0°/-45°/90°)_s$						
III	$(45°/0°/-45°/0°/-45°/90°/0°/45°)_s$						
IV	$(45°/0°/-45°/0°/-45°/0°/45°/0°)_s$						

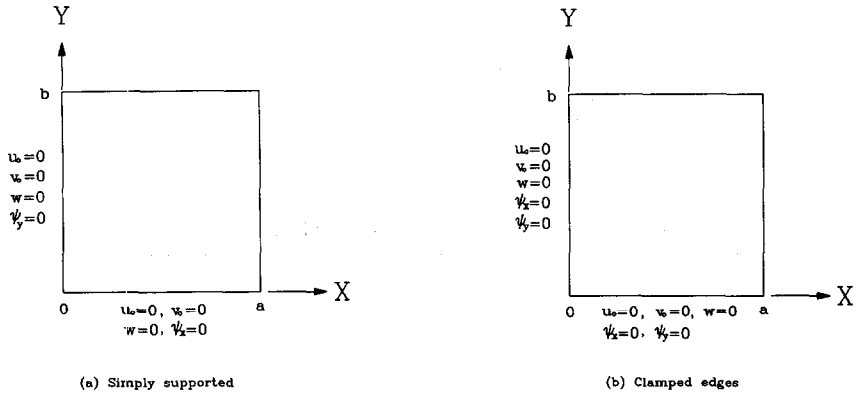

Fig. 4. Boundary conditions of laminated plates subject to uniform load.

Table 4. Deflections of laminated plates subject to uniform load

Boundary condition	Plate	Normalized load $(P/E_2)/(a/h)^4$	Normalized center deflection w_c/h) Present	Reddy and Reddy (1992)
Simply supported	I	9689.1	1.950	1.956
	II	9030.1	1.913	1.919
	III	6177.7	1.842	1.845
	IV	4517.8	1.838	1.840
Clamped	I	5144.9	1.282	1.283
	II	3833.8	1.163	1.164
	III	2442.6	1.055	1.053
	IV	2083.1	1.066	1.064

various lamination arrangements subjected to a uniformly distributed transverse load of intensity P. The properties of the laminates are given in Table 3. The two different boundary conditions and the dimensions of the laminated plates are shown in Fig. 4. In the finite element analysis of the plates, a 4×4 mesh (16 elements over the full plate) of nine-node Lagrangian elements with a 2×2 Gauss integration rule was used to model the laminated plates. The center deflections of the plates subject to a uniform load of various intensities are given in Table 4 and compared with those obtained by Reddy and Reddy (1992) in which a 5×9 mesh of nine-node Lagrangian elements was used in modelling the laminated plates. It is noted that the present finite element method could predict very accurate deflection for the laminated composite plates even when fewer elements are used in the analysis. To validate the capability of the present method in predicting accurate first-ply failure loads, the linear and nonlinear first-ply failure loads of a number of laminated composite plates were determined and compared with those obtained by Reddy and Reddy (1992). Close agreement between the results obtained by the present method and those of Reddy and Reddy (1992) was observed and, furthermore, both methods predicted the same

Table 5. First-ply failure loads of a clamped $[0°/90°]_s$ plate subject to a center point load Q

Failure criterion	Normalized failure load $(Q/E_2)/(a/h)^4$ (I) Present	(II) Reddy and Reddy (1992)	Difference (I) – (II)/(I) %
Maximum stress	159999.5†	160730.7†	0.46
	1151806.2‡	1137201.5‡	1.27
Maximum strain	178368.2	179239.5	0.49
	1577164.3	1549940.9	1.73
Maximum stress (polynomial)	156885.1	157582.2	0.44
	1068028.3	1059047.0	0.84
Maximum strain (polynomial)	174521.2	175345.5	0.47
	1424543.9	1417095.1	0.52
Hoffman	157185.8	157733.4	0.35
	1073394.3	1061680.9	1.09
Tsai–Hill	158314.0	159020.6	0.45
	1092535.2	1083201.5	0.85
Tsai–Wu	169166.1	163416.2	3.40
	1312456.0	1165771.9	11.18

† Linear.
‡ Nonlinear.

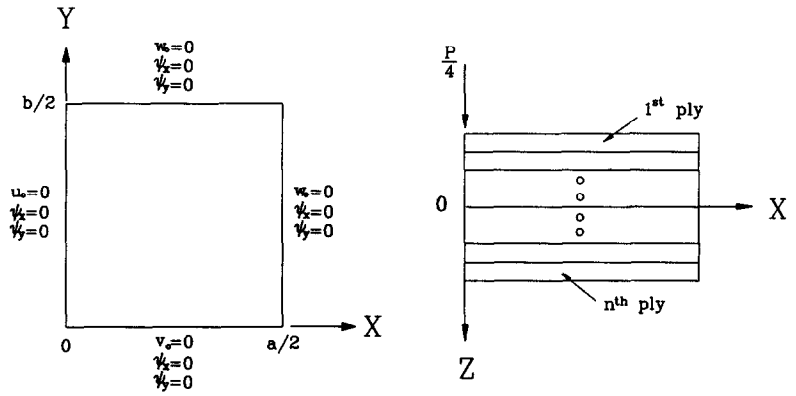

Fig. 5. Boundary conditions of a partially clamped quarter laminated plate.

failure locations. For illustration purposes, Table 5 lists the linear and nonlinear first-ply failure loads of a clamped $[0°/90°]_s$ plate loaded by a center point force predicted by the present method and by Reddy and Reddy (1992) using various failure criteria for comparison. It is noted that in the above analysis the nonlinear first-ply failure load was determined via an incremental–iterative procedure similar to the one adopted by Reddy and Reddy (1992).

The present nonlinear finite element method is then used to predict the deflection and first-ply failure load of four types of partially clamped square thin cross-ply plates, namely, $[0°/90°/0°/90°]_s$, $[0_2°/90_2°]_s$, $[0_2°/90°]_s$ and $[0°/90°]_s$, subject to a center point load. It is worth noting that the contact area between the indentor and the laminated plates is generally small and thus the modeling of the contact force as a concentrated force in the finite element analysis will not affect the overall behavior of the plates if the plates are relatively thin. The boundary conditions of the plates are shown in Fig. 5. A quarter plate is used in the finite element analysis and the results are compared with experimental results (Kam, 1993; Kam and Sher, 1995). First, the effects of the number and type of elements on the finite element load–deflection results are investigated. Figure 6 shows the load–displacement curves of the $[0_2°/90_2°]_s$ plate obtained with the present finite method using different elements (Elements A–C) and a 2×2 mesh compared with the experimental load–displacement curve. It is noted that among the three elements Element C yields the best load–displacement curve when compared with the experimental one. The effect of the number of elements on the accuracy of Element C demonstrated in Fig. 7 is small and in general a 3×3 mesh over a quarter plate yields fairly good results. The effect of boundary conditions on the load–

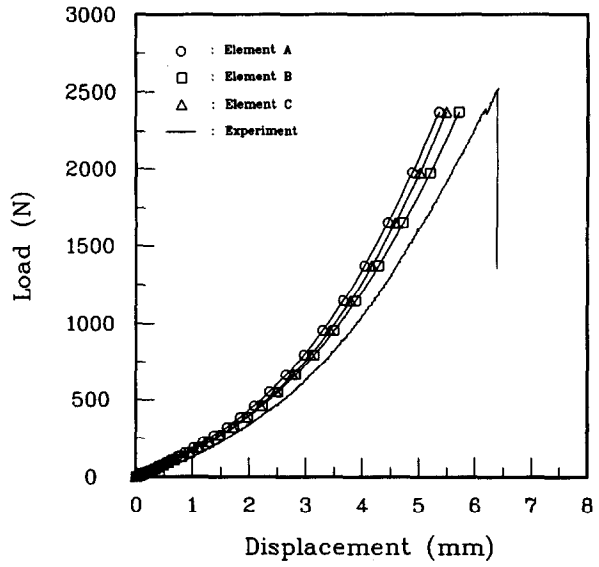

Fig. 6. Load–deflection curves of a $[0_2^\circ/90_2^\circ]_s$ plate modelled by Elements A–C using a 2×2 mesh for a quarter plate without stiffness reduction.

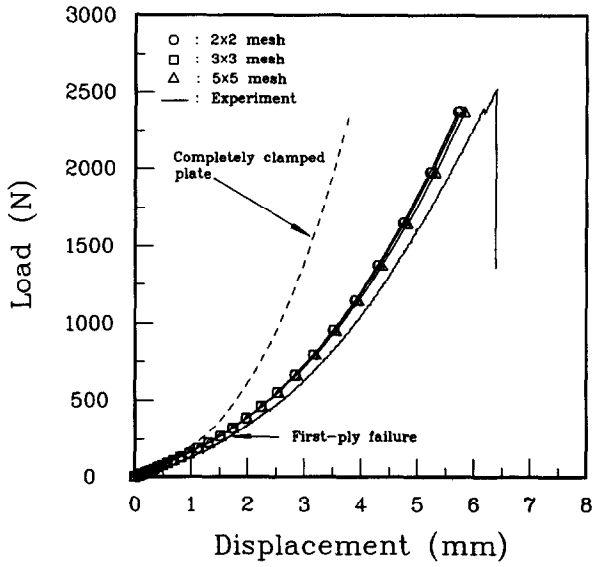

Fig. 7. Load–deflection curves of a $[0_2^\circ/90_2^\circ]_s$ plate modelled by Element C using various meshes for a quarter plate without stiffness reduction.

displacement curve of the $[0_2^\circ/90_2^\circ]_s$ plate is also investigated. The load–displacement curve of the plate with completely clamped edges, i.e. $u_0 = v_0 = w = \psi_x = \psi_y = 0$ along the four edges, using a 3×3 mesh for a quarter plate is plotted in Fig. 7 for comparison. It is noted that the plate with completely clamped edges is much stiffer than the partially clamped one. Next consider the accuracy of the present method with Element C in predicting strains. Strains in the fiber and matrix directions at the center of the bottom surface of the $[0°/90°/0°/90°]_s$ plate under indentation testing were measured using a biaxial strain gauge. Element C with different numbers of elements was used to model the load–strain curves in the fiber and matrix directions for the plate. The experimental and finite element results are shown in Figs 8 and 9 for comparison. It is again noted that the use of a 3×3 mesh over a quarter plate can yield very accurate results. Henceforth, Element C with a 3×3 mesh over a quarter plate is used to study the deflection and strength of cross-ply plates. The load–displacement results for the $[0°/90°/0°/90°]_s$, $[0_2^\circ/90°]_s$ and $[0°/90°]_s$ plates obtained by the present method are shown in Figs 10–12 and compared with the experimental results. It is

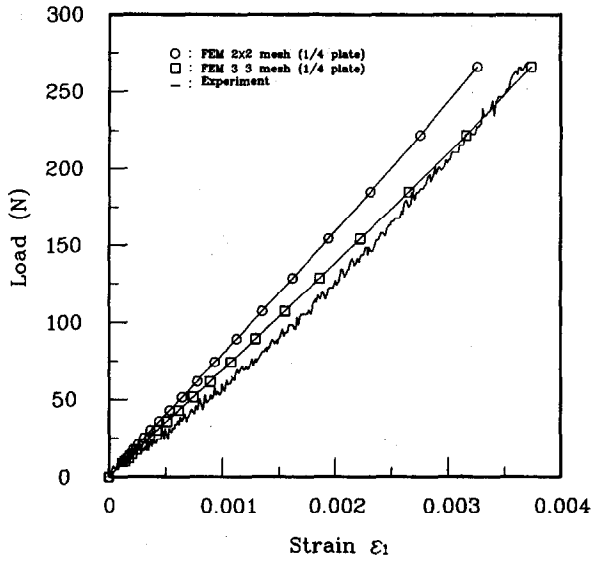

Fig. 8. Analytical and experimental load–strain curves in the fiber direction for a $[0°/90°/0°/90°]_s$ plate.

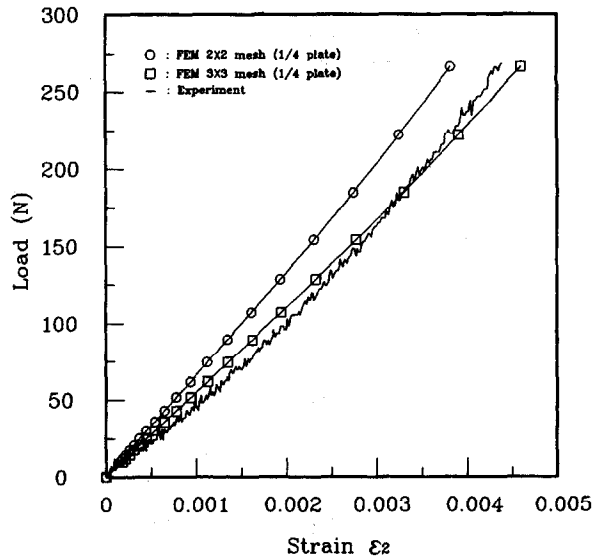

Fig. 9. Analytical and experimental load–strain curves in the matrix direction for a $[0°/90°/0°/90°]_s$ plate.

noted that when compared with the experimental load–displacement curves the present finite element method can yield fairly good load–displacement curves at low loads (before first-ply failure). The discrepancies between the finite element and experimental results at loads higher than the first-ply failure load, which will be determined subsequently, are due to the stiffness reduction of the failed plies. When the aforementioned stiffness reduction model is used with Element C in the deflection analysis of, for instance, $[0_2^\circ/90_2^\circ]_s$ and $[0°/90°/0°/90°]_s$ plates, much better agreement between the analytical and experimental load–displacement curves can be attained as shown in Figs 13 and 14. It is noted that the analytical load–displacement curves of the damaged cross-ply plate have been obtained via a load control type incremental–iterative procedure in which the proposed stiffness reduction model together with an automatic load increment re-sizing technique has been used in tracing the load–displacement curves. The horizontal step changes on the analytical load–displacement curves indicate failures of plies and sudden reductions of plate stiffness. Since the experimental load–displacement curves were obtained via a stroke (displacement)

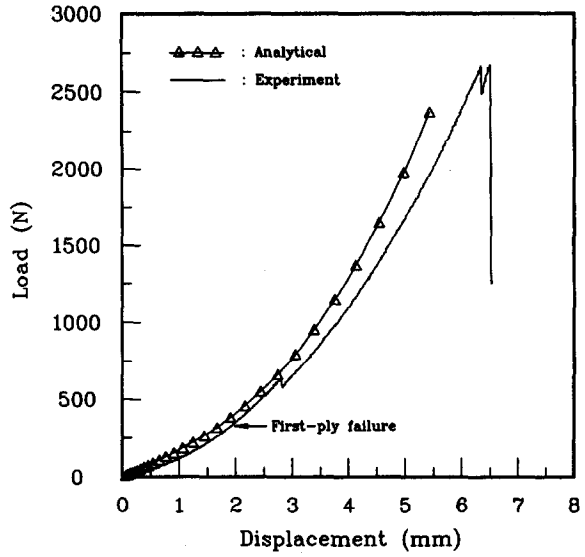

Fig. 10. Analytical and experimental load–deflection curves of a $[0°/90°/0°/90°]_s$ plate without stiffness reduction.

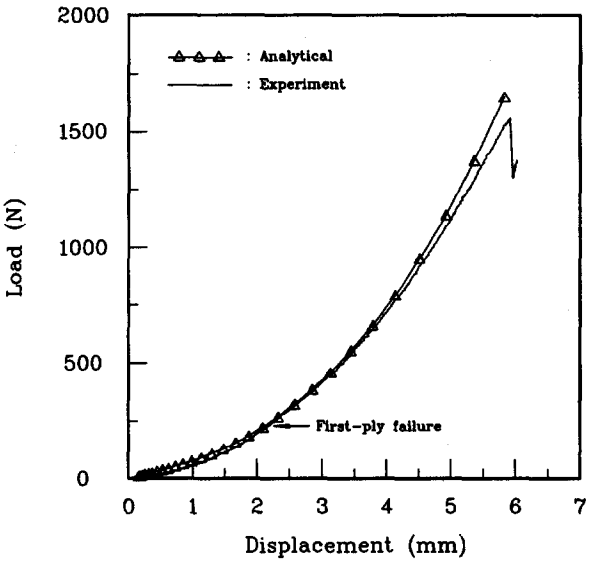

Fig. 11. Analytical and experimental load–deflection curves of a $[0_2^\circ/90°]_s$ plate without stiffness reduction.

control approach, vertical rather than horizontal step changes on the curves could be observed. It is worth pointing out that due to the singularity of the stiffness matrix of a damaged plate under its maximum load, load increments of much smaller sizes have been used to trace the load–displacement curve near the maximum load and the last equilibrium state before the displacement of the plate becomes unbounded is used to approximate the ultimate strength of the plate. Though the use of the proposed maximum stress criterion based stiffness reduction model cannot accurately simulate the failure process of the laminated plates as indicated by the mismatch of the horizontal and vertical step changes in Fig. 14, the ultimate strengths predicted by the finite element method with stiffness reduction may closely approximate the experimental ones with errors less than 15%. Next consider the determination of first-ply failure loads of the laminated composite plates. In Figs 6 and 10–12, the first-ply failure loads cannot be determined directly from either the analytical or experimental load–deflection curves. In the process of estimating the first-ply failure load, the stresses in the plies at the nodes as well as the integration points of each element are first determined in the linear or nonlinear finite element analyses of the plates using Element

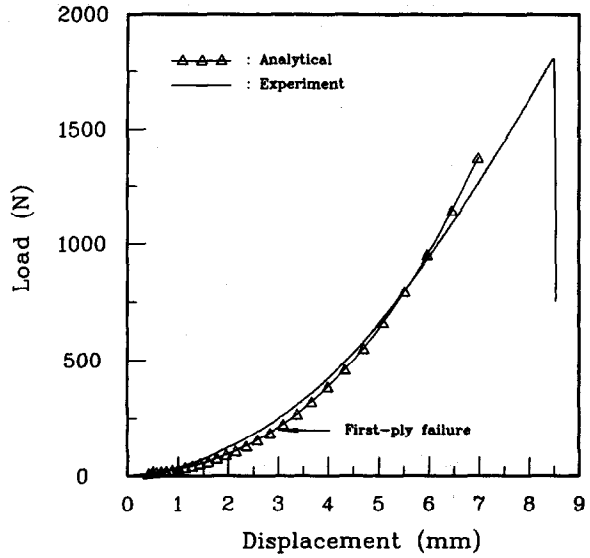

Fig. 12. Analytical and experimental load–deflection curves of a $[0°/90°]_s$ plate without stiffness reduction.

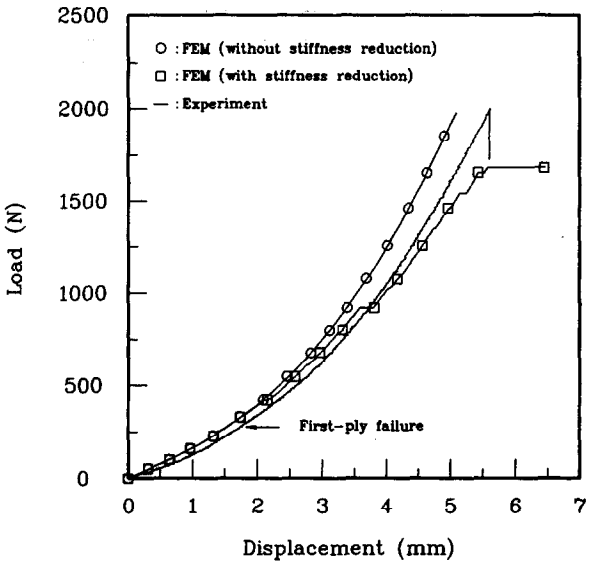

Fig. 13. Load–deflection curves of a $[0_2^\circ/90_2^\circ]_s$ plate with and without stiffness reduction.

C with a 3×3 mesh over a quarter plate. The linear and nonlinear first-ply failure loads for the laminates are then determined using the stresses obtained in the linear and nonlinear finite element analyses, respectively, based on the adopted failure criteria as described in the previous section. The finite element results obtained by the present method are given in Tables 6–9 and compared with the mean experimental results determined from four specimens for each lamination arrangement. The experimental first-ply failure loads of the laminated composite plates were identified directly from the energy vs load charts produced by the AMS3 acoustic emission system as shown, for example, in Fig. 3 for the $[0°/90°/0°/90°]_s$ plate. If the mean experimental first-ply failure loads are treated as exact, the errors in the finite element predictions based on various failure criteria can be determined as indicated in Tables 6–9. Regarding the capabilities of the adopted failure criteria in predicting first-ply failure load, it has been found that the maximum stress (independent and polynomial), Hoffman and Tsai-Hill failure criteria can yield fairly good results with consistent accuracy for the laminated plates. In particular, the independent maximum stress criterion can predict first-ply failure loads with error around 6%. It is also worth noting

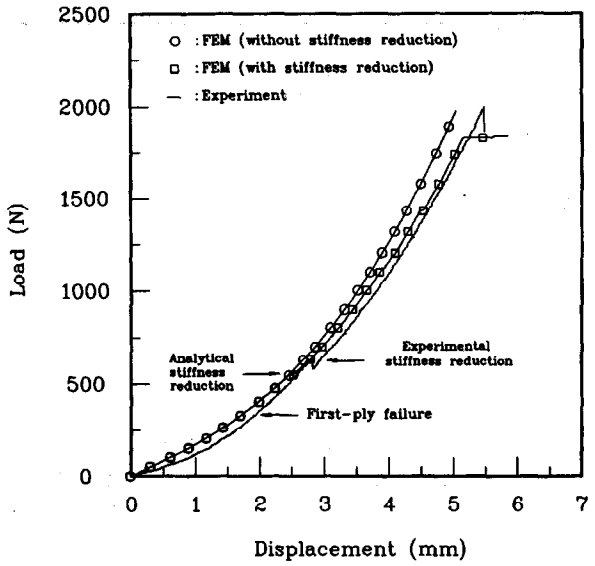

Fig. 14. Load–deflection curves of a $[0°/90°/0°/90°]_s$ plate with and without stiffness reduction.

Table 6. Theoretical and experimental predictions of first-ply failure load for a $[0_2^\circ/90_2^\circ]_s$ plate

Failure criterion	a/h	Theoretical failure load F (N)	Experimental failure load L (N)	Difference $(\lvert F-L\rvert/L)$ %
(i) Maximum stress		229.11†		9.66
		267.08‡		5.32
(ii) Maximum strain		267.55		5.50
		330.91		30.49
(iii) Maximum stress		222.43		12.29
(polynomial)		255.37		0.70§
(iv) Maximum strain	80.645	257.73	253.60	1.63
(polynomial)		312.02		23.04
(v) Hoffman		222.69		12.19
		255.76		0.85
(vi) Tsai-Hill		224.19		11.60
		257.35		1.48
(vii) Tsai-Wu		238.60		5.91
‡		280.44		10.58

†Linear.
‡Nonlinear.
§Minimum error.

that the experimental ultimate failure loads of the plates are much higher than the first-ply failure loads. The capability of simulating the actual failure process and predicting the ultimate failure loads of laminated plates with different lamination arrangements and side-to-thickness ratios is vital in the reliability assessment of such structures. Hence, the importance of the extension of the present method to first-ply failure load and ultimate strength prediction of laminated composite plates is obvious.

8. CONCLUSIONS

A nonlinear finite element method was developed for the prediction of nonlinear load–deflection curves and first-ply failure loads of centrally loaded and partially clamped laminated composite plates using several phenomenological failure criteria. A hypothetical stiffness reduction model was adopted to improve the prediction of load–displacement curves of damaged laminated composite plates. Experimental results on load–displacement curve and first-ply failure load of laminated plates with four different lamination arrangements were used to verify the accuracy of the solutions obtained by the present methods. The results have shown that the present method, especially when used with nine-node

Table 7. Theoretical and experimental predictions of first-ply failure load for a $[0°/90°/0°/90°]_S$ plate

Failure criterion	a/h	Theoretical failure load F (N)	Experimental failure load L (N)	Difference $(\|F-L\|/L)$ %
(i) Maximum stress		290.12†		8.69
		337.26‡		6.14
(ii) Maximum strain		355.47		11.87
		443.07		39.44
(iii) Maximum stress		278.12		12.47
(polynomial)		317.62		0.04§
(iv) Maximum strain	80.645	335.34	317.74	5.54
(polynomial)		405.53		27.57
(v) Hoffman		278.53		12.34
		318.21		0.15
(vi) Tsai–Hill		280.81		11.62
		320.64		0.91
(vii) Tsai–Wu		304.13		4.28
		356.23		12.11

†Linear.
‡Nonlinear.
§Minimum error.

Table 8. Theoretical and experimental predictions of first-ply failure load for a $[0_2^\circ/90°]_s$ plate

Failure criterion	a/h	Theoretical failure load F (N)	Experimental failure load L (N)	Difference $(\|F-L\|/L)$ %
(i) Maximum stress		108.26†		31.19
		147.61‡		6.18
(ii) Maximum strain		122.86		21.91
		185.31		17.78
(iii) Maximum stress		106.34		32.41
(polynomial)		142.92		9.16
(iv) Maximum strain	105.26	120.32	157.34	23.53
(polynomial)		176.84		12.39
(v) Hoffman		106.45		32.34
		143.15		9.02
(vi) Tsai–Hill		107.06		31.96
		144.42		8.21
(vii) Tsai–Wu		112.77		28.33
		157.78		0.28§

†Linear.
‡Nonlinear.
§Minimum error.

Table 9. Theoretical and experimental predictions of first-ply failure load for a $[0°/90°]_s$ plate

Failure criterion	a/h	Theoretical failure load F (N)	Experimental failure load L (N)	Difference $(\|F-L\|/L)$ %
(i) Maximum stress		64.94†		58.92
		150.00‡		5.11§
(ii) Maximum strain		76.04		51.90
		220.35		39.39
(iii) Maximum stress		63.52		59.82
(polynomial)		141.60		10.43
(iv) Maximum strain	152.67	73.99	158.08	53.19
(polynomial)		200.00		26.52
(v) Hoffman		63.60		59.77
		141.96		10.20
(vi) Tsai–Hill		64.03		59.50
		144.06		8.87
(vii) Tsai–Wu		68.30		56.79
		166.40		5.26

†Linear.
‡Nonlinear.
§Minimum error.

Lagrangian elements, can predict fairly good load–deflection curves and ultimate strengths for plates with damage. Nevertheless, the actual failure process of the damaged plates could not be simulated by the present method. Hence, further modification of the proposed stiffness reduction model is required. The capabilities of the phenomenological failure criteria in predicting first-ply failure load have been investigated and discussed. It has been found that fairly accurate determination of first-ply failure loads of laminated composite plates based on maximum stress, Hoffman and Tsai-Hill failure criteria can be achieved. It is suggested that further research on failure mechanisms and predictions of first-ply failure and maximum loads of laminated composite plates subject to transverse loads using other approaches such as fracture energy method be pursued.

Acknowledgement—This research was supported by the National Science Council of the Republic of China under Grant No. NSC 83-0401-E-009-103. Their support is gratefully acknowledged.

REFERENCES

ASTM Standards and Literature References for Composite Material (1990) 2nd Ed.

Cantwell, W. J. and Morton, J. (1985) Detection of impact damage in CFRP laminates. *J. Compos. Structures* **3,** 241–257.

Chang, F. K. and Chang, K. Y. (1987). A progressive damage model for laminated composites containing stress concentrations. *J. Compos. Materials* **21,** 834–855.

Chang, F. K. and Kutlu, Z. (1989). Strength and response of cylindrical composite shells subjected to out-of-plane loadings. *J. Compos. Materials* **23,** 11–31.

Dumir, P. C. and Bhaskar, A. (1988). Nonlinear static analysis of rectangular plates on elastic foundations by the orthogonal point collocation method. *Comput. Meth. Appl. Mech. Engng* **67,** 111–124.

Dvorak, G. J. and Laws, N. (1987). Analysis of progressive matrix cracking in composite laminates II: first ply failure. *J. Compos. Materials* **21,** 309–329.

Garrett, K. W. and Bailey, J. E. (1977). Multiple transverse fracture in 90° cross-ply laminates of a glass fibre-reinforced polyester. *J. Mater. Sci.* **12,** 157–168.

Hahn, H. T. and Tsai, S. W. (1974). On the behavior of composite laminates after initial failure. *J. Compos. Materials* **8,** 288–305.

Highsmith, A. L. and Reifsnider, K. L. (1982). Stiffness–reduction mechanisms in composite laminates. *Damage in Composite Materials*, ASTM ATP 775, pp. 103–117. American Society for Testing and Materials.

Kam, T. Y. (1993). Manufacture of laminated composite materials components, Final Report No. NSC-82-0401-E009-156. National Science Council, Taiwan, R.O.C.

Kam, T. Y. and Lin, S. C. (1992). Reliability analysis of laminated composite plates. *Proc. NSC, Part A*, **16,** 163–171.

Kam, T. Y. and Sher, H. F. (1995). Nonlinear and first-ply failure analyses of laminated composite plates. *J. Compos. Materials* **29,** 463–482.

Kam, T. Y., Lin, S. C. and Hsiao, K. M. (1993). Reliability analysis of nonlinear laminated composite plate structures. *Compos. Structures* **25,** 503–510.

Kuppusamy, T. and Reddy, J. N. (1984). A three-dimensional nonlinear analysis of cross-ply rectangular composite plates. *Comput. Structures* **18,** 263–272.

Laws, N., Dvorak, G. J. and Hejazi, M. (1983). Stiffness changes in unidirectional composites caused by crack systems. *Mech. Materials*, **2,** 123–137.

Reddy, J. N. and Chao, W. C. (1981). Nonlinear bending of thick rectangular laminated plates. *Int. J. Non-linear Mech.* **16,** 291–301.

Reddy, J. N. and Pandey, A. K. (1987) A first-ply failure analysis of composite laminates. *Comput. Structures* **25,** 371–393.

Reddy, Y. S. N. and Reddy, J. N. (1992). Linear and non-linear failure analysis of composite laminates with transverse shear. *Comput. Sci. Tech.* **44,** 227–255.

Talreja, R. (1985). Transverse cracking and stiffness reduction in composite laminates. *J. Compos. Materials* **19,** 355–375.

Tsai, S. W. and Wu, E. M. (1971). A general theory of strength for anisotropic materials. *J. Compos. Materials* **5,** 58–80.

Turvey, G. J. (1980a). An initial flexural failure analysis of symmetrically laminated cross-ply rectangular plates. *Int. J. Solids Structures*, **16,** 451–463.

Turvey, G. J. (1980b). Flexural failure analysis of angle-ply laminates of GFRP and CFRP. *J. Strain Anal.* **15,** 43–49.

Turvey, G. J. (1982). Uniformly loaded, antisymmetric cross-ply laminated, rectangular plates: an initial flexural failure analysis. *Fibre Sci. Technol.* **15,** 1–10.

Turvey, G. J. and Osman, M. Y. (1989). Exact and approximate linear and nonlinear initial failure analysis of laminated Mindlin plates in flexure. *Composite Structures*, Vol. 5 (Edited by I. H. Marshall), pp. 133–171. Elsevier Applied Science, London.

Wang, A. S. D. and Crossman, F. W. (1980). Initiation and growth of transverse cracks and edge delamination in composite laminates, part I. An energy method. *J. Compos. Materials* **14,** 71–87.

APPENDIX A: ELEMENT INTERNAL FORCE VECTOR $F_e = [F_i^\alpha]$

The terms F_i^α ($\alpha = 1, 2, \ldots, 5$, denoting degree of freedom at a node; $i = 1, 2, \ldots, q$, denoting node number) of the element internal force vector F_e are expressed as

$$
\begin{aligned}
F_i^1 = {} & \frac{1}{2}\int_{\Omega_e} A_{11}(2u_{0,x} + w_{0,x}^2)\Phi_{i,x}\,dx\,dy \\
& + \frac{1}{2}\int_{\Omega_e} A_{12}(2v_{0,y} + w_{0,y}^2)\Phi_{i,x}\,dx\,dy \\
& + \frac{1}{2}\int_{\Omega_e} 2A_{16}(w_{0,x}w_{0,y} + u_{0,y} + v_{0,x})\Phi_{i,x}\,dx\,dy \\
& + \frac{1}{2}\int_{\Omega_e} A_{16}(2u_{0,x} + w_{0,x}^2)\Phi_{i,y}\,dx\,dy \\
& + \frac{1}{2}\int_{\Omega_e} A_{26}(2v_{0,y} + w_{0,y}^2)\Phi_{i,y}\,dx\,dy \\
& + \frac{1}{2}\int_{\Omega_e} 2A_{66}(w_{0,x}w_{0,y} + u_{0,y} + v_{0,x})\Phi_{i,y}\,dx\,dy \\
& + \frac{1}{2}\int_{\Omega_e} 2B_{11}\psi_{x,x}\Phi_{i,x}\,dx\,dy \\
& + \frac{1}{2}\int_{\Omega_e} 2B_{12}\psi_{y,y}\Phi_{i,x}\,dx\,dy \\
& + \frac{1}{2}\int_{\Omega_e} 2B_{16}(\psi_{x,y} + \psi_{y,x})\Phi_{i,x}\,dx\,dy \\
& + \frac{1}{2}\int_{\Omega_e} 2B_{26}\psi_{y,y}\Phi_{i,y}\,dx\,dy \\
& + \frac{1}{2}\int_{\Omega_e} 2B_{16}\psi_{x,x}\Phi_{i,y}\,dx\,dy \\
& + \frac{1}{2}\int_{\Omega_e} 2B_{66}(\psi_{x,y} + \psi_{y,x})\Phi_{i,y}\,dx\,dy
\end{aligned}
$$

$$
\begin{aligned}
F_i^2 = {} & \frac{1}{2}\int_{\Omega_e} A_{12}(2u_{0,x} + w_{0,x}^2)\Phi_{i,y}\,dx\,dy \\
& + \frac{1}{2}\int_{\Omega_e} A_{16}(2u_{0,x} + w_{0,x}^2)\Phi_{i,x}\,dx\,dy \\
& + \frac{1}{2}\int_{\Omega_e} 2A_{26}(w_{0,x}w_{0,y} + u_{0,y} + v_{0,x})\Phi_{i,y}\,dx\,dy \\
& + \frac{1}{2}\int_{\Omega_e} A_{26}(2v_{0,y} + w_{0,y}^2)\Phi_{i,x}\,dx\,dy \\
& + \frac{1}{2}\int_{\Omega_e} A_{22}(2v_{0,y} + w_{0,y}^2)\Phi_{i,y}\,dx\,dy \\
& + \frac{1}{2}\int_{\Omega_e} 2A_{66}(w_{0,x}w_{0,y} + u_{0,y} + v_{0,x})\Phi_{i,x}\,dx\,dy \\
& + \frac{1}{2}\int_{\Omega_e} 2B_{12}\psi_{x,x}\Phi_{i,y}\,dx\,dy \\
& + \frac{1}{2}\int_{\Omega_e} 2B_{16}\psi_{x,x}\Phi_{i,x}\,dx\,dy \\
& + \frac{1}{2}\int_{\Omega_e} 2B_{26}(\psi_{x,y} + \psi_{y,x})\Phi_{i,y}\,dx\,dy
\end{aligned}
$$

$$+\frac{1}{2}\int_{\Omega_e} 2B_{26}\psi_{y,y}\Phi_{i,x}\,dx\,dy$$

$$+\frac{1}{2}\int_{\Omega_e} 2B_{22}\psi_{y,y}\Phi_{i,y}\,dx\,dy$$

$$+\frac{1}{2}\int_{\Omega_e} 2B_{66}(\psi_{x,y}+\psi_{y,x})\Phi_{i,x}\,dx\,dy$$

$$F_i^3 = \frac{1}{2}\int_{\Omega_e} A_{11}(2u_{0,x}+w_{0,x}^2)w_{0,x}\Phi_{i,x}\,dx\,dy$$

$$+\frac{1}{2}\int_{\Omega_e} A_{12}(2v_{0,y}+w_{0,y}^2)w_{0,x}\Phi_{i,x}\,dx\,dy$$

$$+\frac{1}{2}\int_{\Omega_e} A_{12}(2u_{0,x}+w_{0,x}^2)w_{0,y}\Phi_{i,y}\,dx\,dy$$

$$+\frac{1}{2}\int_{\Omega_e} 2A_{16}(w_{0,x}w_{0,y}+u_{0,y}+v_{0,x})w_{0,x}\Phi_{i,x}\,dx\,dy$$

$$+\frac{1}{2}\int_{\Omega_e} A_{22}(2v_{0,y}+w_{0,y}^2)w_{0,y}\Phi_{i,y}\,dx\,dy$$

$$+\frac{1}{2}\int_{\Omega_e} 2A_{26}(w_{0,x}w_{0,y}+u_{0,y}+v_{0,x})w_{0,y}\Phi_{i,y}\,dx\,dy$$

$$+\frac{1}{2}\int_{\Omega_e} A_{16}(2u_{0,x}+w_{0,x}^2)w_{0,y}\Phi_{i,x}\,dx\,dy$$

$$+\frac{1}{2}\int_{\Omega_e} A_{16}(2u_{0,x}+w_{0,x}^2)w_{0,x}\Phi_{i,y}\,dx\,dy$$

$$+\frac{1}{2}\int_{\Omega_e} A_{26}(2v_{0,y}+w_{0,y}^2)w_{0,x}\Phi_{i,y}\,dx\,dy$$

$$+\frac{1}{2}\int_{\Omega_e} A_{26}(2v_{0,x}+w_{0,y}^2)w_{0,y}\Phi_{i,x}\,dx\,dy$$

$$+\frac{1}{2}\int_{\Omega_e} 2A_{66}(w_{0,x}w_{0,y}+u_{0,y}+v_{0,x})w_{0,y}\Phi_{i,x}\,dx\,dy$$

$$+\frac{1}{2}\int_{\Omega_e} 2A_{66}(w_{0,x}w_{0,y}+u_{0,y}+v_{0,x})w_{0,x}\Phi_{i,y}\,dx\,dy$$

$$+\frac{1}{2}\int_{\Omega_e} 2B_{11}\psi_{x,x}w_{0,x}\Phi_{i,x}\,dx\,dy$$

$$+\frac{1}{2}\int_{\Omega_e} 2B_{12}\psi_{y,y}w_{0,x}\Phi_{i,x}\,dx\,dy$$

$$+\frac{1}{2}\int_{\Omega_e} 2B_{12}\psi_{x,x}w_{0,y}\Phi_{i,y}\,dx\,dy$$

$$+\frac{1}{2}\int_{\Omega_e} 2B_{16}(\psi_{x,y}+\psi_{y,x})w_{0,x}\Phi_{i,x}\,dx\,dy$$

$$+\frac{1}{2}\int_{\Omega_e} 2B_{22}\psi_{y,y}w_{0,y}\Phi_{i,y}\,dx\,dy$$

$$+\frac{1}{2}\int_{\Omega_e} 2B_{26}(\psi_{y,y}w_{0,y}\Phi_{i,x}+\psi_{y,y}w_{0,x}\Phi_{i,y})\,dx\,dy$$

$$+\frac{1}{2}\int_{\Omega_e} 2B_{16}(\psi_{x,x}w_{0,y}\Phi_{i,x}+\psi_{x,x}w_{0,x}\Phi_{i,y})\,dx\,dy$$

$$+\frac{1}{2}\int_{\Omega_e} 2B_{26}(\psi_{x,y}+\psi_{y,x})w_{0,y}\Phi_{i,y}\,dx\,dy$$

$$+\frac{1}{2}\int_{\Omega_e} 2B_{66}(\psi_{x,y}+\psi_{y,x})(w_{0,y}\Phi_{i,x}+w_{0,x}\Phi_{i,y})\,dx\,dy$$
$$+\frac{1}{2}\int_{\Omega_e} 2A_{55}(\psi_x+w_{0,x})\Phi_{i,x}\,dx\,dy$$
$$+\frac{1}{2}\int_{\Omega_e} 2A_{44}(\psi_y+w_{0,y})\Phi_{i,y}\,dx\,dy$$
$$+\frac{1}{2}\int_{\Omega_e} 2A_{45}[(\psi_x+w_{0,x})\Phi_{i,y}+(\psi_y+w_{0,y})\Phi_{i,x}]\,dx\,dy$$

$$F_i^4=\frac{1}{2}\int_{\Omega_e} 2A_{55}(\psi_x+w_{0,x})\Phi_i\,dx\,dy$$
$$+\frac{1}{2}\int_{\Omega_e} 2A_{45}(\psi_y+w_{0,y})\Phi_i\,dx\,dy$$
$$+\frac{1}{2}\int_{\Omega_e} B_{11}(2u_{0,x}+w_{0,x}^2)\Phi_{i,x}\,dx\,dy$$
$$+\frac{1}{2}\int_{\Omega_e} B_{12}(2v_{0,y}+w_{0,y}^2)\Phi_{i,x}\,dx\,dy$$
$$+\frac{1}{2}\int_{\Omega_e} 2B_{16}(w_{0,x}w_{0,y}+u_{0,y}+v_{0,x})\Phi_{i,x}\,dx\,dy$$
$$+\frac{1}{2}\int_{\Omega_e} B_{16}(2u_{0,x}+w_{0,x}^2)\Phi_{i,y}\,dx\,dy$$
$$+\frac{1}{2}\int_{\Omega_e} B_{26}(2v_{0,y}+w_{0,y}^2)\Phi_{i,y}\,dx\,dy$$
$$+\frac{1}{2}\int_{\Omega_e} 2B_{66}(w_{0,x}w_{0,y}+u_{0,y}+v_{0,x})\Phi_{i,y}\,dx\,dy$$
$$+\frac{1}{2}\int_{\Omega_e} 2D_{11}\psi_{x,x}\Phi_{i,x}\,dx\,dy$$
$$+\frac{1}{2}\int_{\Omega_e} 2D_{12}\psi_{y,y}\Phi_{i,x}\,dx\,dy$$
$$+\frac{1}{2}\int_{\Omega_e} 2D_{16}(\psi_{x,y}+\psi_{y,x})\Phi_{i,x}\,dx\,dy$$
$$+\frac{1}{2}\int_{\Omega_e} 2D_{26}\psi_{y,y}\Phi_{i,y}\,dx\,dy$$
$$+\frac{1}{2}\int_{\Omega_e} 2D_{16}\psi_{x,x}\Phi_{i,y}\,dx\,dy$$
$$+\frac{1}{2}\int_{\Omega_e} 2D_{66}(\psi_{x,y}+\psi_{y,x})\Phi_{i,y}\,dx\,dy$$

$$F_i^5=\frac{1}{2}\int_{\Omega_e} 2A_{44}(\psi_y+w_{0,y})\Phi_i\,dx\,dy$$
$$+\frac{1}{2}\int_{\Omega_e} 2A_{45}(\psi_x+w_{0,x})\Phi_i\,dx\,dy$$
$$+\frac{1}{2}\int_{\Omega_e} B_{22}(2v_{0,y}+w_{0,y}^2)\Phi_{i,y}\,dx\,dy$$
$$+\frac{1}{2}\int_{\Omega_e} B_{12}(2u_{0,x}+w_{0,x}^2)\Phi_{i,y}\,dx\,dy$$
$$+\frac{1}{2}\int_{\Omega_e} 2B_{26}(w_{0,x}w_{0,y}+u_{0,y}+v_{0,x})\Phi_{i,y}\,dx\,dy$$

$$+\frac{1}{2}\int_{\Omega_e} B_{26}(2v_{0,y}+w_{0,y}^2)\Phi_{i,x}\,dx\,dy$$

$$+\frac{1}{2}\int_{\Omega_e} B_{16}(2u_{0,x}+w_{0,x}^2)\Phi_{i,x}\,dx\,dy$$

$$+\frac{1}{2}\int_{\Omega_e} 2B_{66}(w_{0,x}w_{0,y}+u_{0,y}+v_{0,x})\Phi_{i,x}\,dx\,dy$$

$$+\frac{1}{2}\int_{\Omega_e} 2D_{22}\psi_{y,y}\Phi_{i,y}\,dx\,dy$$

$$+\frac{1}{2}\int_{\Omega_e} 2D_{12}\psi_{x,x}\Phi_{i,y}\,dx\,dy$$

$$+\frac{1}{2}\int_{\Omega_e} 2D_{26}(\psi_{x,y}+\psi_{y,x})\Phi_{i,y}\,dx\,dy$$

$$+\frac{1}{2}\int_{\Omega_e} 2D_{26}\psi_{y,y}\Phi_{i,x}\,dx\,dy$$

$$+\frac{1}{2}\int_{\Omega_e} 2D_{66}(\psi_{x,y}+\psi_{y,x})\Phi_{i,x}\,dx\,dy$$

$$+\frac{1}{2}\int_{\Omega_e} 2D_{16}\psi_{x,x}\Phi_{i,x}\,dx\,dy.$$

APPENDIX B: ELEMENT TANGENT STIFFNESS MATRIX $\mathbf{K}_e = [K_{ij}^{\alpha\beta}]$

The terms $K_{ij}^{\alpha\beta}$ ($\alpha, \beta = 1, 2, \ldots, 5$, denoting degree of freedom at a node; $i, j = 1, 2, \ldots, q$, denoting node number) of the element tangent stiffness matrix $\mathbf{K}_e$ are given by

$$K_{ij}^{11} = A_{11}S_{ij}^{x}+A_{16}(S_{ij}^{xy}+S_{ji}^{xy})+A_{66}S_{ij}^{y}$$

$$K_{ij}^{12} = A_{12}S_{ij}^{xy}+A_{16}S_{ij}^{x}+A_{26}S_{ij}^{y}+A_{66}S_{ji}^{xy}$$

$$K_{ij}^{13} = 2[A_{11}R_{xij}^{x}+A_{12}R_{yij}^{xy}+A_{16}(R_{xij}^{yx}+R_{yij}^{x}+R_{xij}^{xy})+A_{26}R_{yij}^{y}+A_{66}(R_{yij}^{yx}+R_{xij}^{y})]$$

$$K_{ij}^{31} = 2[A_{11}R_{xij}^{x}+A_{12}R_{yij}^{yx}+A_{16}(R_{xij}^{xy}+R_{yij}^{x}+R_{xij}^{yx})+A_{26}R_{yij}^{y}+A_{66}(R_{yij}^{xy}+R_{xij}^{y})] = [K_{ij}^{13}]^{\mathrm{T}}$$

$$K_{ij}^{23} = 2[A_{12}R_{xij}^{yx}+A_{22}R_{yij}^{y}+A_{26}(R_{xij}^{y}+R_{yij}^{yx}+R_{yij}^{xy})+A_{66}(R_{yij}^{x}+R_{xij}^{xy})+A_{16}R_{xij}^{x}]$$

$$K_{ij}^{32} = 2[A_{12}R_{xij}^{xy}+A_{22}R_{yij}^{y}+A_{26}(R_{xij}^{y}+R_{yij}^{xy}+R_{yij}^{yx})+A_{66}(R_{yij}^{x}+R_{xij}^{yx})+A_{16}R_{xij}^{x}] = [K_{ij}^{23}]^{\mathrm{T}}$$

$$K_{ij}^{14} = B_{11}S_{ij}^{x}+B_{16}(S_{ij}^{xy}+S_{ji}^{xy})+B_{66}S_{ij}^{y} = [K_{ij}^{41}]^{\mathrm{T}}$$

$$K_{ij}^{15} = B_{12}S_{ij}^{xy}+B_{16}S_{ij}^{xy}+B_{26}S_{ji}^{xy}+B_{66}S_{ji}^{y} = [K_{ij}^{51}]^{\mathrm{T}}$$

$$K_{ij}^{22} = A_{26}(S_{ij}^{xy}+S_{ji}^{xy})+A_{22}S_{ij}^{y}+A_{66}S_{ij}^{x}$$

$$K_{ij}^{24} = B_{16}S_{ij}^{x}+B_{66}S_{ij}^{xy}+B_{12}S_{ij}^{xy}+B_{26}S_{ij}^{y} = [K_{ij}^{42}]^{\mathrm{T}}$$

$$K_{ij}^{25} = B_{26}(S_{ij}^{xy}+S_{ji}^{xy})+B_{22}S_{ij}^{y}+B_{66}S_{ij}^{x} = = [K_{ij}^{52}]^{\mathrm{T}}$$

$$K_{ij}^{33} = e_1^2S_{ij}^{x}+e_2^2S_{ij}^{y}+e_1e_2(S_{ij}^{xy}+S_{ji}^{xy})$$
$$+\frac{1}{2}\int_{\Omega_e} A_{11}(2u_{0,x}+3w_{0,x}^2)\Phi_{i,x}\Phi_{j,x}\,dx\,dy$$
$$+\frac{1}{2}\int_{\Omega_e} A_{12}(2v_{0,y}+w_{0,y}^2)\Phi_{i,x}\Phi_{j,x}\,dx\,dy$$
$$+\frac{1}{2}\int_{\Omega_e} A_{12}(2u_{0,x}+w_{0,x}^2)\Phi_{i,y}\Phi_{j,y}\,dx\,dy$$

$$+\frac{1}{2}\int_{\Omega_e} A_{16}(6w_{0,x}w_{0,y}+2u_{0,y}+2v_{0,x})\Phi_{i,x}\Phi_{j,x}\,dx\,dy$$

$$+\frac{1}{2}\int_{\Omega_e} A_{22}(2v_{0,y}+3w_{0,y}^2)\Phi_{i,y}\Phi_{j,y}\,dx\,dy$$

$$+\frac{1}{2}\int_{\Omega_e} A_{26}(6w_{0,x}w_{0,y}+2u_{0,y}+2v_{0,x})\Phi_{i,y}\Phi_{j,y}\,dx\,dy$$

$$+\frac{1}{2}\int_{\Omega_e} 2A_{12}w_{0,x}w_{0,y}(\Phi_{i,x}\Phi_{j,y}+\Phi_{i,y}\Phi_{j,x})\,dx\,dy$$

$$+\frac{1}{2}\int_{\Omega_e} A_{16}(2u_{0,x}+3w_{0,x}^2)(\Phi_{i,x}\Phi_{j,y}+\Phi_{i,y}\Phi_{j,x})\,dx\,dy$$

$$+\frac{1}{2}\int_{\Omega_e} A_{26}(2v_{0,y}+3w_{0,y}^2)(\Phi_{i,x}\Phi_{j,y}+\Phi_{i,y}\Phi_{j,x})\,dx\,dy$$

$$+\frac{1}{2}\int_{\Omega_e} A_{66}(4w_{0,x}w_{0,y}+2u_{0,y}+2v_{0,x})(\Phi_{i,x}\Phi_{j,y}+\Phi_{i,y}\Phi_{j,x})\,dx\,dy$$

$$+\frac{1}{2}\int_{\Omega_e} 2B_{11}\psi_{x,x}\Phi_{i,x}\Phi_{j,x}\,dx\,dy$$

$$+\frac{1}{2}\int_{\Omega_e} 2B_{12}\psi_{y,y}\Phi_{i,x}\Phi_{j,x}\,dx\,dy$$

$$+\frac{1}{2}\int_{\Omega_e} 2B_{12}\psi_{x,x}\Phi_{i,y}\Phi_{j,y}\,dx\,dy$$

$$+\frac{1}{2}\int_{\Omega_e} 2B_{16}(\psi_{x,x}+\psi_{y,y})\Phi_{i,x}\Phi_{j,x}\,dx\,dy$$

$$+\frac{1}{2}\int_{\Omega_e} 2B_{22}\psi_{y,y}\Phi_{i,y}\Phi_{j,y}\,dx\,dy$$

$$+\frac{1}{2}\int_{\Omega_e} 2B_{26}(\psi_{x,x}+\psi_{y,y})\Phi_{i,y}\Phi_{j,y}\,dx\,dy$$

$$+\frac{1}{2}\int_{\Omega_e} 2B_{16}\psi_{x,x}(\Phi_{i,x}\Phi_{j,y}+\Phi_{i,y}\Phi_{j,x})\,dx\,dy$$

$$+\frac{1}{2}\int_{\Omega_e} 2B_{26}\psi_{y,y}(\Phi_{i,x}\Phi_{j,y}+\Phi_{i,y}\Phi_{j,x})\,dx\,dy$$

$$+\frac{1}{2}\int_{\Omega_e} 2B_{66}(\psi_{x,y}+\psi_{y,x})(\Phi_{i,x}\Phi_{j,y}+\Phi_{i,y}\Phi_{j,x})\,dx\,dy$$

$$K_{ij}^{34}=e_1^2S_{ij}^{x0}+e_1e_2S_{ij}^{y0}+2[B_{11}R_{xij}^{x}+B_{12}R_{yij}^{yx}+B_{16}(R_{xij}^{yx}+R_{yij}^{x}+R_{xij}^{xy})+B_{26}R_{yij}^{y}+B_{66}(R_{yij}^{xy}+R_{xij}^{y})]$$

$$K_{ij}^{43}=e_1^2S_{ij}^{0x}+e_1e_2S_{ij}^{0y}+2[B_{11}R_{xij}^{x}+B_{12}R_{yij}^{xy}+B_{16}(R_{xij}^{yx}+R_{yij}^{x}+R_{xij}^{xy})+B_{26}R_{yij}^{y}+B_{66}(R_{yij}^{yx}+R_{xij}^{y})]$$

$$K_{ij}^{35}=e_2^2S_{ij}^{y0}+e_1e_2S_{ij}^{x0}+2[B_{12}R_{xij}^{xy}+B_{16}R_{xij}^{x}+B_{26}(R_{yij}^{yx}+R_{yij}^{xy}+R_{xij}^{y})+B_{22}R_{yij}^{y}+B_{66}(R_{yij}^{x}+R_{xij}^{yx})]$$

$$K_{ij}^{53}=e_2^2S_{ij}^{0y}+e_1e_2S_{ij}^{0x}+2[B_{12}R_{xij}^{yx}+B_{16}R_{xij}^{x}+B_{26}(R_{yij}^{xy}+R_{yij}^{yx}+R_{xij}^{y})+B_{22}R_{yij}^{y}+B_{66}(R_{yij}^{x}+R_{xij}^{xy})]$$

$$K_{ij}^{44}=D_{11}S_{ij}^{x}+D_{16}(S_{ij}^{xy}+S_{ji}^{xy})+D_{66}S_{ij}^{y}+e_1^2S_{ij}^{0}$$

$$K_{ij}^{45}=D_{12}S_{ij}^{xy}+D_{66}S_{ij}^{yx}+D_{26}S_{ij}^{y}+D_{16}S_{ij}^{x}+e_1e_2S_{ij}^{0}=[K_{ij}^{54}]^{\mathrm{T}}$$

$$K_{ij}^{55}=D_{26}(S_{ij}^{xy}+S_{ji}^{xy})+D_{66}S_{ij}^{x}+D_{22}S_{ij}^{y}+e_2^2S_{ij}^{0},$$

where

$$S_{ij}^{\xi\zeta}=\int_{\Omega_e}\Phi_{i,\xi}\Phi_{j,\zeta}\,d\xi\,d\zeta,\quad(\xi,\zeta=0,x,y)$$

$$R_{\eta ij}^{\xi\zeta}=\frac{1}{2}\int_{\Omega_e} w_{0,\eta}\Phi_{i,\xi}\Phi_{j,\xi}\,d\xi\,d\zeta,\quad(\eta,\xi,\zeta=0,x,y)$$

$$\Phi_{i,0}=\Phi_i,\ S_{ij}^{\xi 0}=S_{ij}^{\xi},\ R_{\eta ij}^{\xi 0}=R_{\eta ij}^{\xi}$$

$$e_1^2=k_1^2\bar{A}_{55},\ e_1e_2=k_1k_2\bar{A}_{45},\ e_2^2=k_2^2\bar{A}_{44}.$$